Pulsed magnetic flux leakage method for hairline crack detection and characterization.

Chukwunonso K. Okolo and Turgut Meydan, [a)]

Wolfson Centre for Magnetics, School of Engineering, Cardiff University, Cardiff, CF24 3AA, UK.

The Magnetic Flux leakage (MFL) method is a well-established branch of electromagnetic Non-Destructive Testing (NDT), extensively used for evaluating defects both on the surface and far-surface of pipeline structures. However the conventional techniques are not capable of estimating their approximate size, location and orientation, hence an additional transducer is required to provide the extra information needed. This research is aimed at solving the inevitable problem of granular bond separation which occurs during manufacturing, leaving pipeline structures with miniature cracks. It reports on a quantitative approach based on the Pulsed Magnetic Flux Leakage (PMFL) method, for the detection and characterization of the signals produced by tangentially oriented rectangular surface and far-surface hairline cracks. This was achieved through visualization and 3D imaging of the leakage field. The investigation compared finite element numerical simulation with experimental data. Experiments were carried out using a 10mm thick low carbon steel plate containing artificial hairline cracks with various depth sizes, and different features were extracted from the transient signal. The influence of sensor lift-off and pulse width variation on the magnetic field distribution which affects the detection capability of various hairline cracks located at different depths in the specimen is explored. The findings show that the proposed technique can be used to classify both surface and far-surface hairline cracks and can form the basis for an enhanced hairline crack detection and characterization for pipeline health monitoring.

I. INTRODUCTION.

A defect is an irregularity or variance from the initial structure of the pipeline. This could be a modification in the wall thickness due to missing metals or as a result of the pipe wall being deformed. However, a crack is a defect type caused by stress-induced separation of the material. Steel materials are made up of granules which are strongly bonded together, however, different factors can result in these strong granular bonds detaching from each other, resulting in the formation of cracks which grow over time. One such factor is the cyclic fatigue. This refers to the pipe stress that develops from the rise and fall of the pipe's operating pressure, which causes a slight change in the shape of the pipe, leading to a gradual weakening and cracking of the pipe[1]. Sometimes, during manufacturing, cracks are accidentally created in pipelines which are initially too minute and insignificant to cause a breakdown but can grow into larger cracks over time, capable of threatening the integrity of the pipe [1].

Magnetic Flux Leakage (MFL) inspection is a non-contact form of Non-Destructive Testing (NDT) used for examining pipeline structures for the presence of defects and imperfections such as: cracks, corrosion, pits, dents, shrinkages, voids, etc [2, 3]. It is the most reliable, efficient and widely used approach for detecting cracks present in both the axial and circumferential directions [4]. The technique is more powerful compared to the eddy current method in terms of the variation of magnetic properties in magnetic materials [5]. MFL method have been in existence as a notable technique for pipeline health monitoring since the 1960's [6, 7]. In the introductory phase, the sensing system used were magnetic powders, which outputs its test results by accumulating at the defective region. The technique is direct, easy, and highly sensitive and has been extensively used in the petrochemical, oil and gas industries. Since the evolution of the semiconductor electronic industries, magnetic sensors such as; GMR, AMR and Hall Effect sensors have achieved enormous breakthrough. It has been proven that the sensitivity of the MFL inspection is improved while using the magnetic field sensor compared to the coil sensor for detecting MFL signals, also the conventional coil sensor system is not very sensitive to low frequency field, where the electromotive force developed around the loop is equivalent to the rate of change of the field, instead of the field magnitude. Hence the coils performance reduces as frequency decreases. The use of magnetic sensor arrays for MFL probes have been developed and have shown better prospect for acquiring more information regarding the orientation and position of defect via mapping of the magnetic field distribution as well as producing a better depth information [8, 9]. More information is attainable at a particular time with the sensor array topology, hence the detection probability is enhanced. This eliminated the drawbacks of measuring devices like magnetic powder and coil sensors. MFL inspection does not require pre-processing and the resulting leakage signal are simple to detect and distinguish. Online based detection can be comfortably achieved and a high degree of automation can be realized. MFL inspection is not limited to assessing the internal surfaces for flaws but can also assess external surfaces for far-surface flaws [10]. The required conditions for the detection environment are not many and they are not disturbed by the transportation medium. These numerous advantages confirms why the MFL testing method is the most popular and widely used NDT technique [4, 11]. Since the introduction of the MFL method in the early 60's, it has grown from the simple recognition of flaws in components and assemblies to the quantitative investigation stage [12, 13]. In spite of some promising theoretical and experimental accomplishments that has been established, the method is not completely accurate. Some of the major drawbacks of the MFL

[a]Corresponding Author: T. Meydan, Email address: Meydan@cardiff.ac.uk

inspection are that: a lot of qualitative study of the resulting signal is required that the MFL method is seldom employed in practice, since the real intricate problems, complex working conditions and requirements can't be compared to the laboratory conditions [14, 15]. It is very sensitive to the moving speed of the motor. Further study and analysis is required to develop a quantitative description of flaws and no direct correlation exists between the signal characteristics and depth of the flaw. The limited crack depth information offered by the conventional MFL methods makes the interpretation of the leakage signals from far-surface cracks difficult.

There are three different techniques of MFL excitation, this includes; direct current (DCMFL) method, alternating current (ACMFL) method and pulsed current (PMFL) method [5, 16]. The DCMFL approach employs the use of an electro magnet to produce a static magnetization field for the magnetization of the test sample. The electromagnet based DCMFL technique is well suited for hard-magnetization materials, like steel pipelines, since the supply current can be varied to provide the large currents required to generate a strong magnetization field. However, this technique does not provide sufficient data, in terms of the defect location and size. The defect has to happen on just one side of the test sample to enable an accurate extraction of the defect features. Frequent demagnetization is required in order to completely cancel out the residual magnetism developed from previous scans, so as to ensure an MFL signal which is comparatively constant and repeatable for successive scans. Depending on the excitation frequency selected, the ACMFL method is usually sensitive to surface and near surface flaws due to skin effect. The ACMFL method is well suited for detecting surface flaws, such as corrosions and cracks in pipeline structures. The PMFL method is a new electromagnetic NDT method which incorporate both the testing technology of eddy current testing and magnetic flux leakage testing. The PMFL method can provide more information needed for defect depth characterization through time/frequency domain analysis of the induced signal, and can be used to determine the position of surface and far-surface defects using the amplitude of the resultant leakage signal. Hence, it provides an added advantage over the traditional MFL methods [5]. Also, with a good signal processing technique and data analysis, further information such as the defect profile can be ascertained. The PMFL probe is operated using a pulsed current or voltage as the excitation signal, while the rich frequency components generates information from various depths due to skin effect. Advancement in the accuracy of MFL technique is required in numerous applications, such as in the pipeline inspection service industries, where satisfactory accuracy in crack detection and quantification can prevent needless costly pipe replacement. Hence a Pulsed MFL method is proposed in this paper, to detect and characterize tangentially oriented hairline cracks both on the surface and far-surface of pipeline structures. The remaining sections of this paper is organized as follows. Section 2 describes the PMFL principle. Section 3 presents the Finite element computation of PMFL numerical models on tangential oriented cracks. Section 4 presents the finite element results. Section 5 describes the experimental methodology used for the PMFL investigation. Section 6 shows the experimental result and discussion which shows a good correlation with the predicted results. Section 7 describes the future work.

II. PRINCIPLE OF PMFL TESTING.

The PMFL inspection principle is simple. It employs the use of a pulsed voltage or current loaded on an excitation coil wounded around an excitation yoke, to obtain a partial magnetization of the test sample. The presence of a crack on a magnetized sample will disturb the initial flow of flux, since the permeability of the defective part will be lower than that of the non-defective parts, resulting in an increase in the magnetic reluctance. This will force the flux to take a different path (path with least resistance) and a leakage flux will build up at the defective part. Subsequently, some flux will leak away from the defective part into the surrounding air. The leakage flux is measured using an appropriate magnetic field sensor positioned perpendicular to the field orientation and within close proximity to the crack. The distribution pattern of the leakage field will be influenced by the ratio of the crack depth to the sample wall thickness, width, length and sharpness at the edges [17]. The PMFL probe is driven with a square waveform, with a constant duty cycle. The excitation signal contains a range of frequency components that delivers the deeper penetration depth of low-frequency excitation (50Hz) and the sensitivity to surface and far-surface measurements of high-frequency excitation (10 kHz) [12]. The penetration depth also known as the skin depth $\boldsymbol{\delta_o}$ is governed by skin effect which is defined as the depth below the surface of a conductive sample at which the current density (J) has reduced to 1/e (about 37%) of the current density at the surface $\boldsymbol{J_s}$ [18]. The skin depth $\boldsymbol{\delta_o}$ can be determined from equation (1).

$$\delta_o = \sqrt{\frac{2}{w\mu\sigma}} \tag{1}$$

Where, $\boldsymbol{\sigma}$ is the electrical conductivity (S/m) of the material used, $\boldsymbol{\omega} = 2\pi f$ is the angular velocity and **f** is the operating frequency. This equation can also be used to determine the desired frequency required to penetrate the conductive material. This means that samples with large thickness could be investigated for far-surface cracks while still maintaining a good sensitivity for surface cracks.

III. FINITE ELELMENT COMPUTATION.

Finite element modelling (FEM) is commonly used in the study and analysis of electromagnetic methods [19]. FEM can effectively predict the field pattern in the vicinity of a crack, thus providing a good platform for designing an optimized PMFL probe system. In this work, MagNet 7.6 software by Infolytica is used to model a 3D non-linear system to investigate the influence of surface and far-surface hairline cracks on the magnetic field distribution, and to predict the response of a PMFL probe scanned above a hairline crack. The three stages involved in analyzing the magnetic field using the finite element analysis software (MagNet) are: (a) the pre-processing stage (construction of model components, Physical properties of components, model units, element type, specification of current, boundary conditions and meshing), (b) solving stage (magnetostatic, time harmonic, time transient) and, (c) post-processing (contour, shaded or arrow plots). Fig. 1 shows a PMFL inspection probe setup used for this investigation. The probe system was modelled as a full model and solved as a 3D problem. The efficiency of the system has been assessed for the detection of both surface and far-surface hairline cracks, with different depth sizes, on a 10mm thick carbon steel plate. The following Maxwell's equations is used with their usual conventional representation and relevant boundary conditions.

$$\nabla . B = 0 \quad (2)$$

$$\nabla \times H = J \quad (3)$$

$$\nabla \times A = B \quad (4)$$

$$\mathrm{B} = \mu_0 \mu_r H = \mu_0 H + \mu_0 M \quad (5)$$

Boundary conditions are utilized and set in a region sufficiently larger than the region of interest in order not to affect the result (see Fig. 1a). A smaller mesh size of 0.02 mm is used at the inside and outside regions of the crack in order to achieve accurate results (see Fig. 1c). The crack is made at the 0 mm mark (centre of sample) and positioned perpendicular to the applied magnetization field. Seven samples with surface cracks of varying depth sizes (d = 0.2, 0.4, 0.6, 0.8, 1, 2, and 4 mm), and seven samples with far-surface cracks of varying depth sizes (d = 0.2, 0.4, 0.6, 0.8, 1, 2, and 4 mm) were tested. All the cracks used in this investigation has a constant width and length of 0.2 mm and 10 mm respectively. The depth of the surface cracks refers to the distance from the top surface of the sample to the bottom tip of the crack, while the depth of the far-surface cracks refers to the distance from the bottom surface of the sample to the top tip of the crack with an opening at the bottom of the sample (see Fig. 1d and 1e). The far-surface cracks are located 9.8, 9.6, 9.4, 9.2, 9, 8 and 6 mm below the top surface of the samples. The dimension of the sample used is $350\ mm \times 60\ mm \times 10\ mm$ with a conductivity of 1.17×10^7 S/m. The excitation yoke (silicon iron) used has a leg height of 80 mm, leg length of 30 mm, leg width of 60 mm, leg spacing of 240 mm with a conductivity of 2.17×10^6 S/m. The yoke was wound with 300 turns of copper wire with a diameter and conductivity of 0.5 mm and 1.12×10^7 S/m respectively. This setup is used to predict the axial (B_x) component of the leakage field for both the surface and far-surface cracks. The excitation coil is driven with a square waveform and is fed with a 4 V amplitude voltage, 500 ms period, 50% duty cycle and the rise and fall time is set to $10\ ns$. The transient responses are obtained when the field probe is directly above a crack with a sensor lift-off of 0.5 mm. Multiple load steps is used in the solver to ensure an accurate calculated results. The positive full cycle of the PMFL inspection model is analyzed and the distribution pattern of the axial (B_x) component of the leakage signal is acquired for different pulse periods. However, the 500 ms period gave the best result. The computational time for the simulation took 55 mins in a dual-core 64-bit processor workstation with 24 GB primary memory.

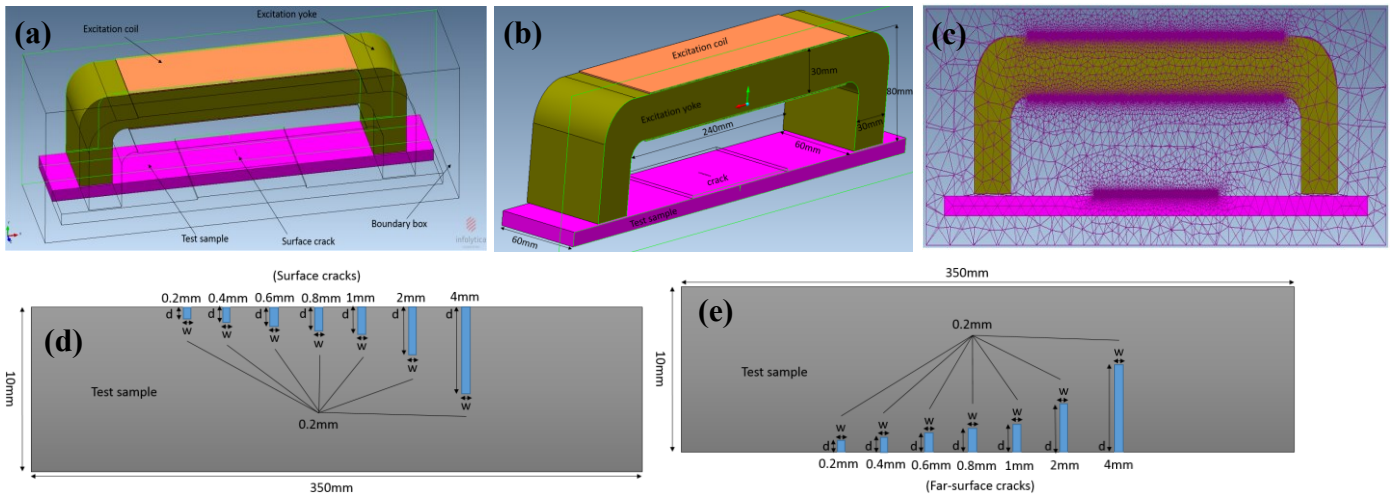

Fig. 1. FEM schematic layout showing; a) PMFL probe setup alongside crack, b) PMFL probe with dimensions, c) Meshed simulation model, d) Test sample with surface cracks and e) Test sample with far-surface cracks.

IV. FINITE ELEMENT RESULTS.

In order to obtain the crack features from the pulse signals, the method of first differential approach is employed. If b and b_0 are two samples with the same magnetic properties and physical size, except that sample b has a crack while b_0 does not. The differential crack signal $\Delta B_{xb} = B_{xb} - B_{xb_0}$ is acquired, where B_{xb} is the disturbance field generated by a crack (crack signal) and B_{xb_0} is the base value from a crack free region (reference signal). Fig. 2 shows the predicted axial (B_x) component of the leakage field obtained at the center of various hairline cracks for the whole time interval. It compares the leakage field from both surface cracks (see Fig. 2a) and far-surface cracks (see Fig 2b) with different depth sizes, using the differential crack signals (ΔB_{xb}). In all the plots used, the excitation pulse starts to rise at t = 0 ms. It can be seen from the plots that the presence of either a surface or far-surface crack causes a significant increase in the signal amplitude. The change in signal amplitude for both kinds of crack is similar for the same change in crack depth, except that the overall signal level is lower for the far-surface cracks. It is also evident from both plots that the PMFL model can clearly discriminate between the depths of the various cracks as well as their location by using the amplitudes of the resultant signals. The FEM model was able to detect a 0.2 mm deep far-surface hairline crack located 9.8 mm below the sample surface, and could discriminate between a 0.2 mm surface and 0.2 mm far-surface cracks.

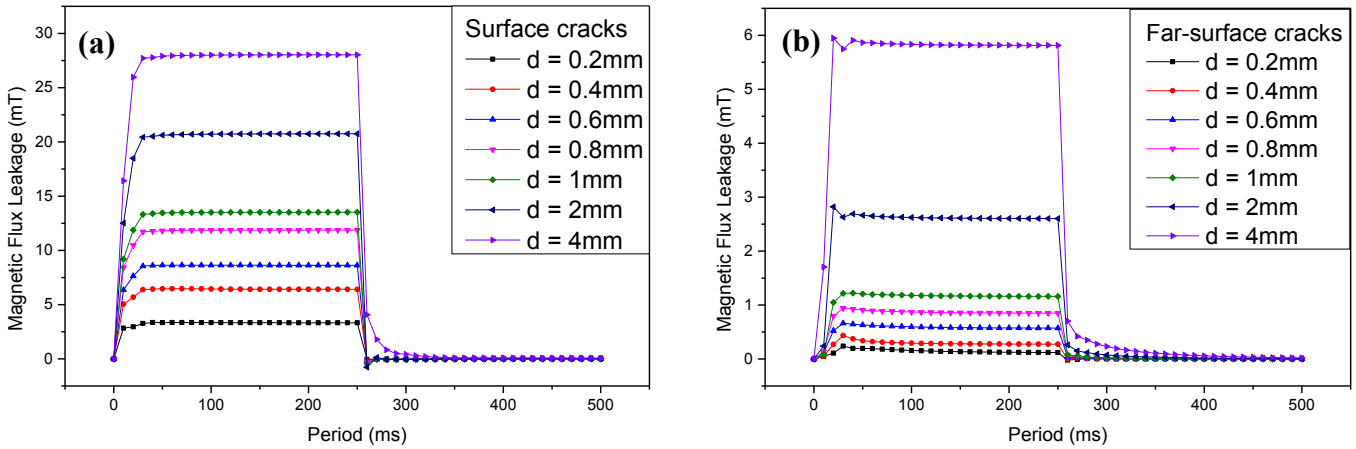

Fig. 2. Time domain representation - Showing the predicted differential crack signal (ΔB_{xb}) as a function of time for; a) Surface cracks and b) Far-surface cracks.

V. EXPERIMENTAL SETUP.

An experimental PMFL investigation is performed to explore the practicality of the PMFL probe system designed using the FEM package, for tangential hairline crack detection and characterization. The yoke was wound with 300 turns of a firm double-coated and high thermally durable copper wire with a diameter of 0.5 mm and resistance of 1.02 Ω. A square waveform of 4 V amplitude and 500 ms period, with a duty cycle of 50% was used for the driver coil excitation. The samples used have cracks with different depth locations ranging from 0.2 mm to 4 mm with a constant width and length of 0.2 mm and 10 mm respectively. The probe position is maintained for all the measurements. The complete test set-up used for the experimental investigation is shown in Fig. 3. Measurements were made by scanning a single Hall Effect sensor (A1302KUA-T) across the cracks, within a scanning distance of 100 mm, in steps of 0.1 mm, and with a constant sensor lift-off of 0.5 mm. x = 0 is the central major axis of the crack. The Hall Effect sensor used has a sensitivity of 1.377 mV/G. The sensor is positioned perpendicular to the orientation of the crack, and held in place by a 3D printed sensor holder attached to an x-y-z translation stage. The axial (B_x) component of the PMFL signal is measured using the Hall sensor and a data acquisition system (NI USB-6366) with 16-bit analogue to digital conversion card is used to digitize the filtered output from the sensor and then stored in a computer for signal processing. A current sensor is incorporated in the probe system in other to measure the amount of current that is fed into the excitation coil. A LabVIEW interface is used to visualize data and communicate with the motors and sensor electronics. For each scanning cycle, data were collected at 1000 samples per second.

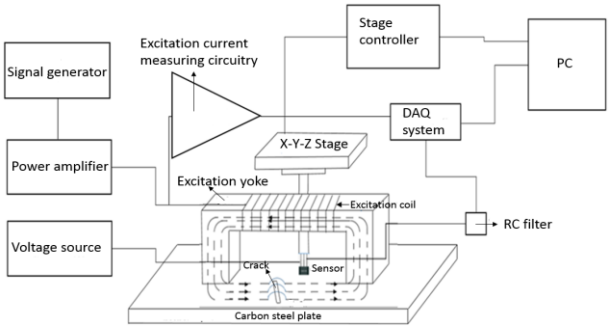

Fig. 3. Showing the PMFL experimental probe system set-up.

VI. EXPERIMENTAL RESULTS AND DISCUSSION.

For a crack which spreads deep into the sample, the penetration depth of the magnetic field have to be enough to yield a comprehensive crack detection and characterization. The leakage field amplitude is strongly dependent on the crack shape. Especially, the peak amplitude of leakage field distribution with respect to the axial distance, is highly dependent on crack depth and position.

A. Crack Characterization.

The distinctive response of the PMFL probe to a 4mm deep surface crack (40% wall loss) is shown in Fig. 4a (crack signal) and 4b (differential crack signal). The unit of percent is expressed as the ratio of defect depth to the sample wall thickness. The plot points out the distinctive change in the pulse shape as the sensor approaches the crack. It can be seen that the leakage signal measured for both the crack signal and differential crack signal varies with relative position of the PMFL sensor to the crack axis, with the highest signal amplitude recorded at the crack centre. The plot clearly shows the distortion of the rising edge of the pulse as the sensor approaches the crack. The plot also shows the peaks and troughs on both sides of the ends of the crack. The increase in field along the sides of the crack is a good indicator of the position of the crack in the x direction mostly around the ends. Fig. 5 is a typical plot of the measured axial (B_x) component of the leakage fields acquired at the centre of each hairline crack. It shows the calculated differential crack signals (ΔB_{xb}) obtained from both surface cracks (see Fig. 5a), and far-surface cracks (see Fig. 5b) as a function of scanning distance. The result clearly shows that as the percentage of the metal loss increases, the peak amplitude of the axial flux increases for cracks of identical width and length. This shows that the leakage flux in the axial direction is strongly dependent on the ratio of crack depth to wall thickness. Also, the broader signal width observed for the far-surface cracks when compared to an equivalent surface crack is attributed to the lateral spread of magnetic field at the vicinity of the far-surface cracks. Fig. 6 shows the measured axial (B_x) component of the leakage field obtained at the centre of various hairline cracks for the whole time interval. The excitation pulse starts to rise at t = 0 ms. It compares the leakage fields from both surface cracks (see Fig. 6a) and far-surface cracks (see Fig. 6b) with different depth sizes, using the acquired differential crack signals (ΔB_{xb}). The information displayed shows that the presence of either a surface or far-surface crack causes a significant increase in the amplitude of the leakage signal measured. It is also evident from the plot that the variation in leakage field as a result of a shallow surface defect and a deep far-surface defect can be discriminated. The system is able to discriminate between a 0.4 mm deep surface crack and a 0.4 mm deep far-surface crack located 9.6 mm below the sample surface. The system can also discriminate between a 0.6 mm, 0.8 mm, 2 mm and 4 mm surface and far-surface cracks. However, it is not able to clearly discriminate between a 0.2 mm surface and 0.2 mm far-surface cracks. Fig. 7 compares the peak amplitudes of the leakage field from both surface and far-surface cracks (2%, 4%, 6%, 8%, 10%, 20% and 40% crack depth to wall thickness) obtained at the centre of each crack, and at t = 150 ms. The behaviour of the leakage field for both the crack signal (B_{xb}^{Peak}) and differential crack signal (ΔB_{xb}^{Peak}) is similar. However, the amplitude of the leakage field for the crack signal is higher than that of the differential crack signal. It can be seen that the amplitude of the leakage field increases as the crack depth increases from left to right, and the relationship between the intensity of leakage field and the crack depth is linearly dependent. The plot shows that the axial component (B_x) of the leakage field provides good information about the position of cracks, by analysing the peak points as the sensor moves across the crack. This also shows that the amplitude of the signal measured by the sensor is proportional to the depth of the crack when the length and width are unchanged. The excitation period of 150 ms used for the characterization of the various hairline cracks as shown in Fig. 6 and Fig. 7, based on their different ΔB_{xb} amplitude, is long compared to the complete magnetization of the sample, such that the results obtained will be similar to the DC field results. However the advantage of the pulsed method used in this case is a significant reduction in the power consumption and thermal effects for hairline crack detection and characterization, compared with the constant powering of the excitation yoke and coil (DCMFL). Hence

eliminating the need to cool the excitation coil for longer inspection period. The experimental PMFL probe system used is able to detect a 0.4 mm deep far-surface hairline crack located 9.6 mm below the sample surface, with a good signal to noise ratio. However it is not able to detect a 0.2 mm far-surface crack located 9.8 mm below the sample surface.

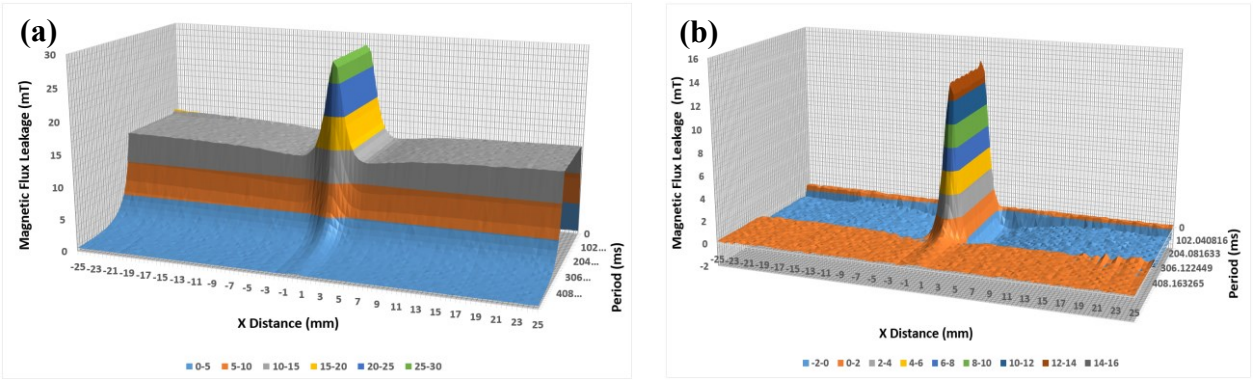

Fig. 4. Time domain representation - Showing the measured axial (B_x) component of the leakage field for a 4 mm deep surface hairline crack; a) Crack signal and b) Differential Crack signal.

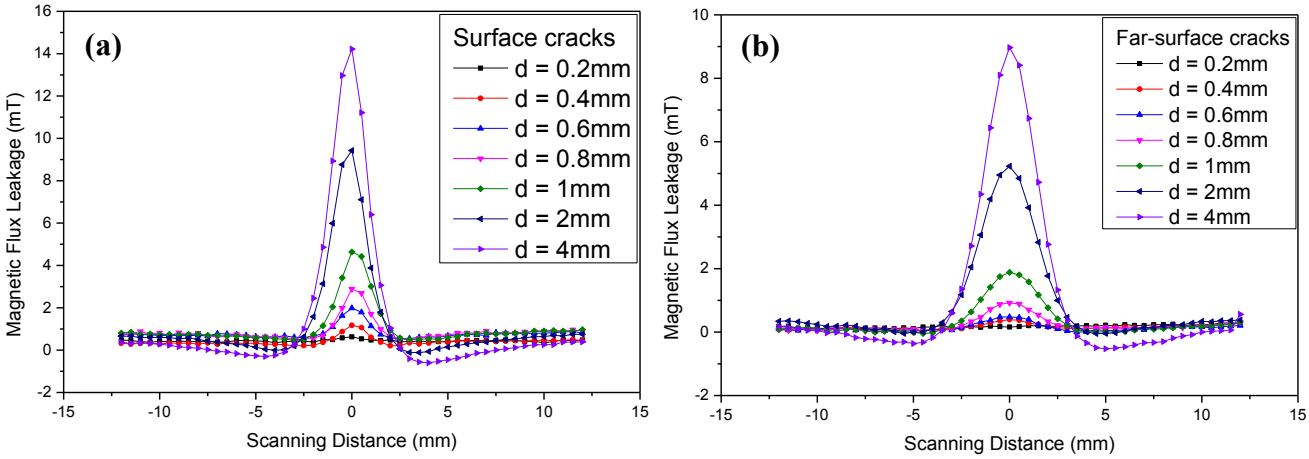

Fig. 5. Showing the measured differential crack signal (ΔB_{xb}) obtained at the center of each crack, as a function of crack position for; a) Surface cracks and b) Far-surface cracks.

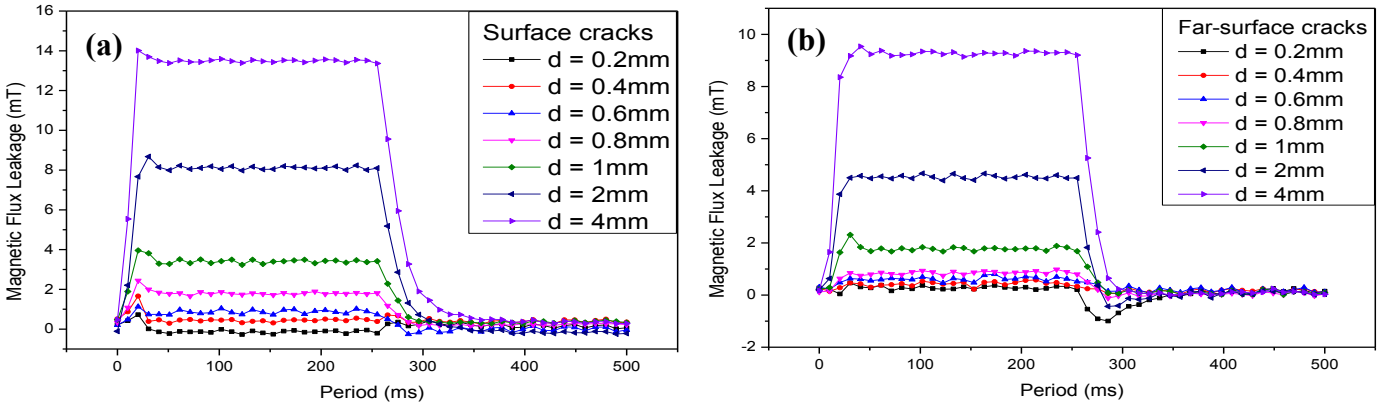

Fig. 6. Time domain representation - Showing the measured differential crack signal (ΔB_{xb}) obtained at the center of each crack, as a function of time for; a) Surface cracks and b) Far-surface cracks.

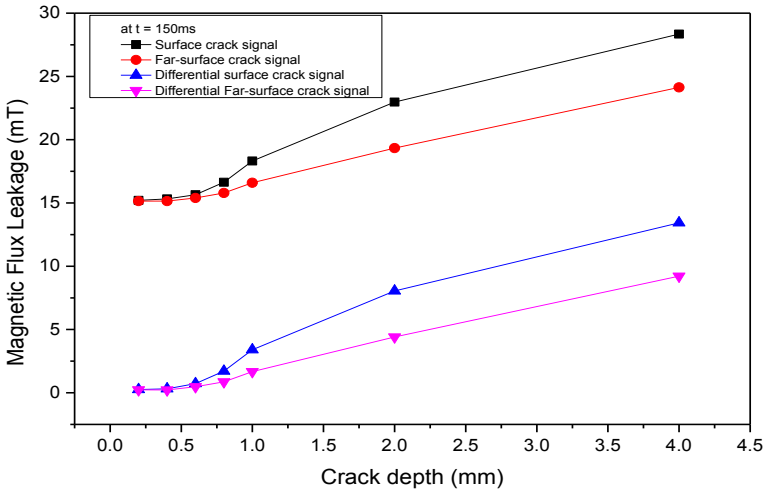

Fig. 7. Showing the peak amplitudes of the measured crack signals (B_{xb}) and differential crack signals (ΔB_{xb}) for various hairline cracks with varying depth sizes at **t = 150ms**. (Obtained at the centre of each crack).

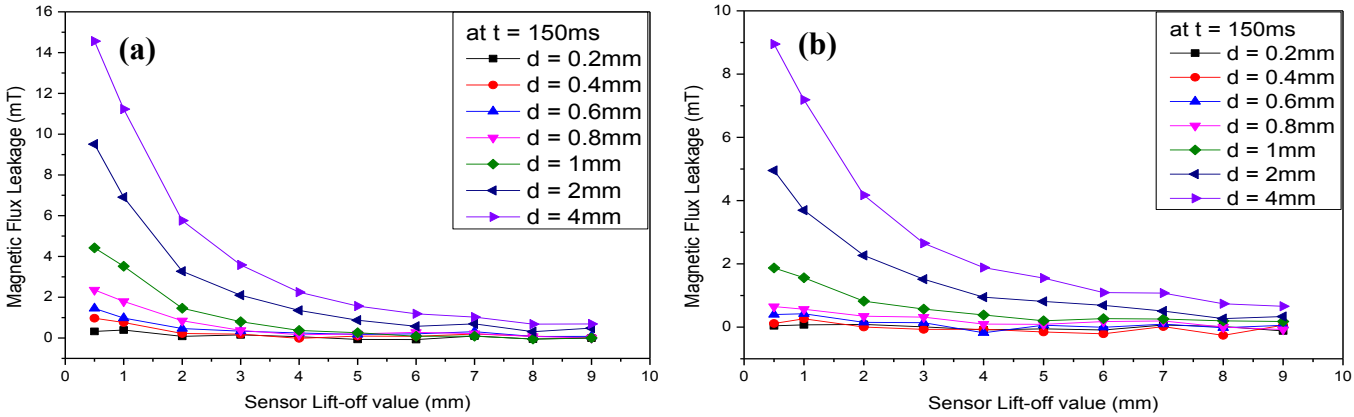

Fig. 8. Showing the relationship between the differential crack signal (ΔB_{xb}^{Peak}) and crack depth at different lift-off values; a) Surface cracks and b) Far-surface cracks

B. Influence of Sensor Lift-off.

The sensor lift-off was varied from 0.5mm to 9mm in other to investigate the effect of sensor lift-off on the detectability of surface and far-surface hairline cracks. Fig. 8 shows the relationship between the acquired peak amplitude of differential crack signal (ΔB_{xb}^{Peak}) and the depth of various surface (see Fig. 8a) and far-surface (see Fig.8b) cracks, at various sensor lift-off values. As expected, the amplitude of the differential crack signal for both the surface and far-surface cracks weakens as the lift-off value of the test probe increases. Also the rate of decrease of the signal amplitude as the lift-off value increases was observed to be more for the surface cracks as compared to the far-surface cracks. This means that the lift-off effect caused by welds and debris during pipeline inspection could result in inaccurate measurement of the true magnitude of the leakage signal which could lead to cracks being missed or undersized, especially for hairline cracks. Also a greater percentage change in the reduction of (ΔB_{xb}^{Peak}) amplitude was observed at lower levels of sensor lift-offs when compared to higher levels of sensor lift-offs. The PMFL sensor maintained a high sensitivity to a 4 mm deep surface and far-surface cracks at a lift-off distance of 9 mm.

C. Influence of Pulse Width Variation.

The pulse width variation technique improves the crack detection capability as well as broadens the preceding PMFL investigation by utilizing pulses with various pulse width, with a constant period. This aids in the recognition of the pulse width that provides the best magnetic field distribution and penetration depth. Eight different pulse widths; (5 ms, 10 ms, 25 ms, 50 ms, 100 ms, 150 ms, 200 ms, and 250 ms) were investigated, which is equivalent to 1%, 2%, 5%, 10%, 20%, 30%, 40% and 50% duty cycles. The

excitation current input fed into the magnetization coil at different pulse widths, while using a sample without a crack is shown in Fig. 9. The result shows that the current amplitude reaches its peak at the 100 ms pulse width corresponding to 20% duty cycle. Fig.10 shows the acquired differential crack signal (ΔB_{xb}^{Peak}) obtained from a 100 mm line scan across a 4mm deep surface crack as a function of time, for excitation waveforms 1%, 2%, 5%, 10%, 20%, 30%, 40% and 50% duty cycles. The result shows that the amplitude of the leakage field increases as the pulse width increases. Also, all the eight pulse widths investigated were able to show a clear indication of the 4mm deep surface crack inspected. Fig.11 shows the acquired differential crack signal (ΔB_{xb}) obtained from a 100mm line scan across a 4mm deep far-surface crack located 6mm below the sample surface as a function of time, at different pulse widths. The various pulse widths investigated were able to show an indication of the 4mm deep far-surface crack inspected, except for the 5ms pulse width, corresponding to 1% duty cycle. However, increasing the pulse width provides a clear indication of the crack position and orientation, without any reduction in sensitivity to surface crack detection. This is because the induced magnetic field in the excitation cycle possess a variation of frequency components at various time intervals, which corresponds to different depth of penetration of the induced field at different points in the cycle. This means that samples with large thickness could be investigated for far-surface cracks using longer pulse widths, while still maintaining a good sensitivity for surface cracks. Also the broader signal width observed at the far-surface crack region when compared to the surface crack of the same size, is attributed to the spreading out of magnetic field at the far-surface crack region.

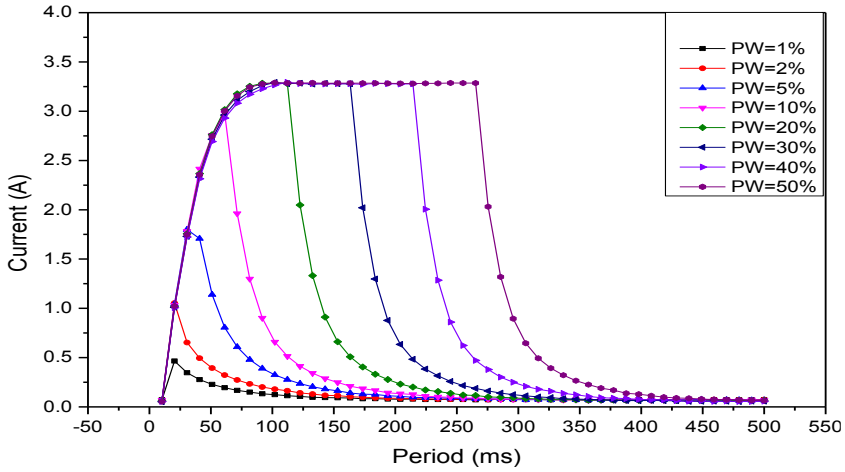

Fig. 9. Time domain representation - Showing the excitation current input flowing inside the coil at different pulse widths.

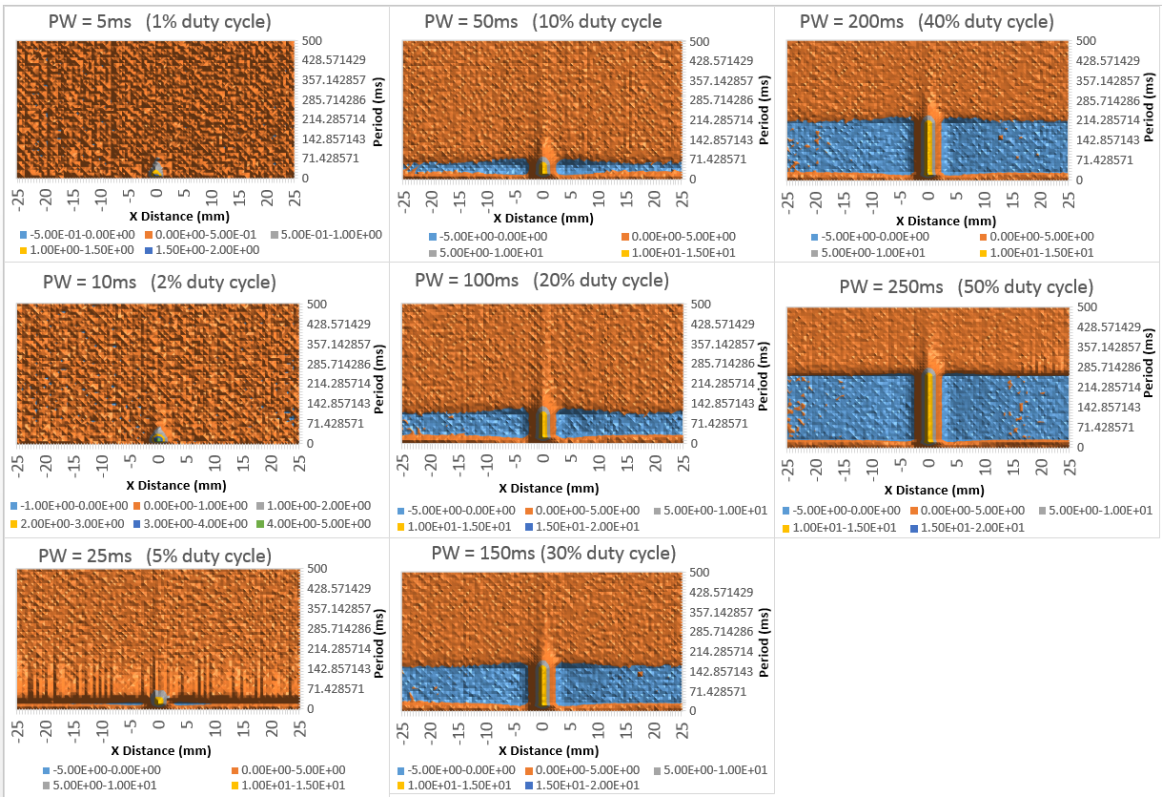

Fig.10. Showing a line scan of the differential crack signal obtained in the vicinity of a 4mm deep surface crack at different pulse width.

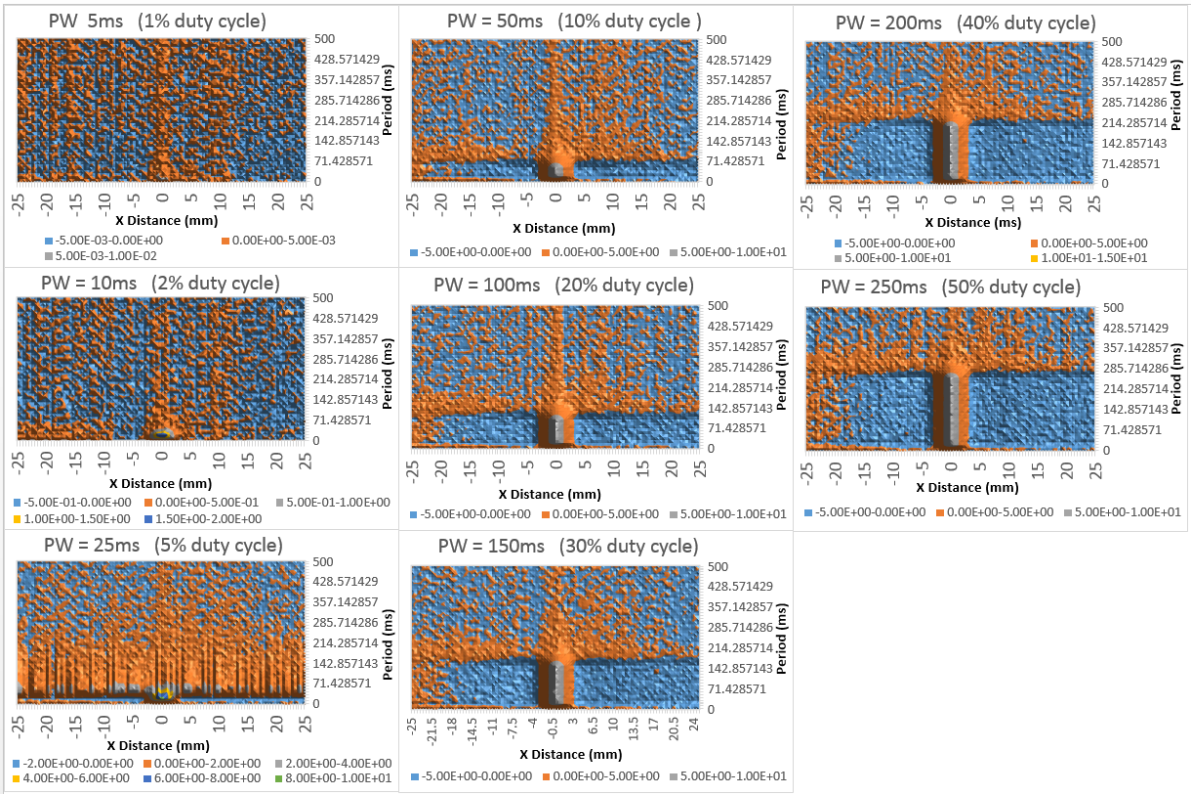

Fig.11. Showing a line scan of the differential crack signal obtained in the vicinity of a 4mm deep far-surface crack at different pulse widths.

D. Crack Width and Length Estimation.

The typical response of the PMFL sensor in the axial (B_x) direction for a 4mm deep surface hairline crack and a 4mm deep far-surface hairline crack is displayed in Fig. 12a and 12b respectively. The scanned area presented is a surface of 24 mm × 24 mm, with a constant scan step size of 0.1 mm in the x and y directions. A square waveform of 4 V amplitude and 500 ms period, with a duty cycle of 20% corresponding to 100 ms pulse width was used for the driver coil excitation. A method based on visualization and 3D imaging of the resultant leakage signal is proposed in order to obtain the approximate width and length of various hairline cracks present in ferromagnetic pipeline structures using the differential crack signal (ΔB_{xb}) . The leakage field distribution with respect to the sensing path distance for the 4 mm deep surface crack and 4mm deep far-surface crack is shown in Fig 12c and 12d respectively. It can be seen that the approximate width and length of both types of cracks inspected can be extracted from the leakage field signals in the width and length directions respectively. The broader signal width observed for the far-surface crack when compared to the surface crack of the same size is attributed to the lateral spread of the leakage field in the vicinity of the far-surface crack. However it is challenging to determine the actual depth of the cracks from the signal width, because the signal width is hardly changed by the variation in crack depth as shown in Fig. 5. The 100 ms pulse width used was found to be very effective in detecting both cracks, which means more energy could be saved while still maintaining a good detection sensitivity to both surface and far-surface cracks. Thus improving the efficiency of the PMFL system for Quantitative non-destructive testing.

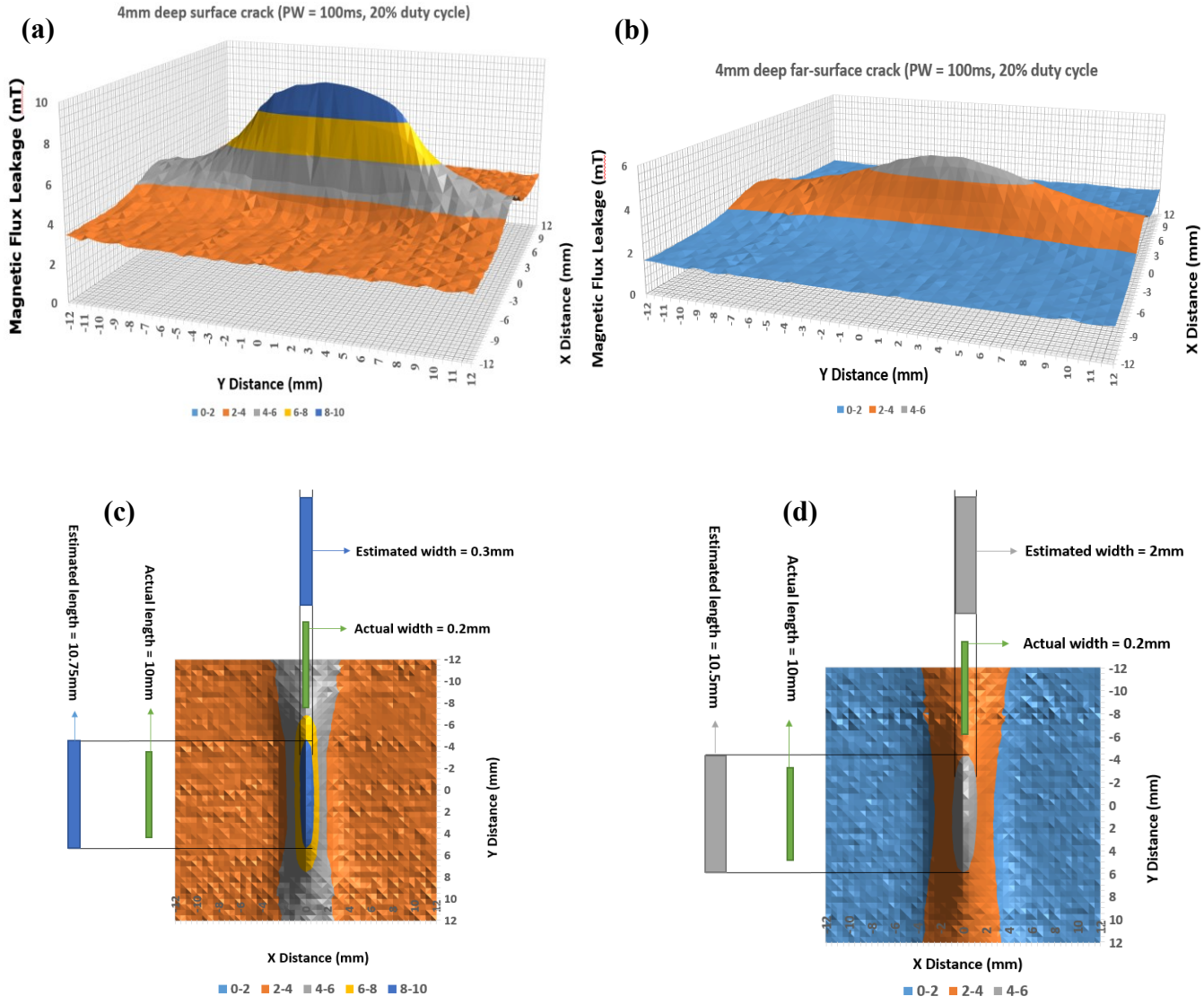

Fig. 12. Showing the measured axial (B_x) component of the leakage field for; a) 4mm deep surface crack, b) 4mm deep far-surface crack: top view of the axial (B_x) component of the leakage field for; c) 4mm deep surface crack and d) 4mm deep far-surface crack.

VII. CONCLUSION.

This paper has used the finite element analysis software, MagNet by Infolytica to model a pulse magnetic flux leakage probe system capable of predicting the resultant leakage field due to surface and far-surface hairline cracks. The accuracy and practicality of the FEM system was assessed for the detection of surface and far-surface hairline cracks on a 10mm thick low carbon steel sample using an experimental approach. The amplitude of the measured signals as well as the analysis of the acquired differential signal which was calculated by subtracting the signal from a crack free region from the signal from a crack region, were used as vital elements in characterizing the various hairline cracks. It was found that the modelled PMFL probe was able to enhance the detection sensitivity of the PMFL system by detecting a 4 mm deep surface hairline crack and 0.2 mm deep far-surface hairline crack located 9.8 mm below the sample surface. Depth information for surface crack up to 4 mm deep was obtained from the signals via experiments, but the deepest far-surface crack for which depth information could be extracted was 0.4 mm, located 9.6mm below the sample surface. Both the FEM and experimental methods were able to discriminate between a shallow surface crack and a deep far-surface crack. The leakage field peak amplitude was found to be strongly determined by the crack depth, a slight variation in depth causes a significant change in the leakage field peak value. The experimental result showed that the leakage signal amplitude is sensitive to the sensor lift-off and an inverse relationship exists between the differential crack signal and the sensor lift-off. A greater percentage change in reduction of the leakage field was observed at lower levels of sensor lift-off when compared to higher lift-off values. Also the rate of decrease of the signal amplitude as the lift-off value increases was observed to be more for the surface cracks as compared to the far-surface cracks.This means that welds and debris existing on the surface of pipeline structures can result to a false interpretation of the leakage signal amplitude especially for hairline cracks, thus reducing the quality of PMFL inspection data and the overall integrity assessment. The system showed a good sensitivity to a 4 mm deep surface and 4 mm deep far-surface hairline cracks at a lift-off distance of 9 mm. PMFL experimental investigation with different pulse widths of constant period was performed in order to investigate the influence of pulse width variation on the distribution of magnetic field within the sample. The low and high frequency components contained in the pulse spectrum was found to provide the PMFL method additional flexibility for crack examination and characterization by using the rich frequency components to separate cracks that exist at the sample surface from those deep below the sample surface. The experimental result show that the approximate length and width of both the surface and far-surface cracks could be obtained from the width of the differential crack signal along the width and length directions respectively. However the far-surface crack exhibited a broader signal profile due to the lateral spread of leakage field at the far-surface region.

Finally, a general guidance has been established for a model-based optimization and experimental investigation using the PMFL method of NDT for effective detection and characterization of hairline cracks in ferromagnetic pipeline structures. This will also enable an effective detection and monitoring of hairline surface and far-surface cracks resulting from the inevitable granular bond separation which occurs during manufacturing leaving pipeline structures with miniature cracks. Future work will involve the development of a 3-axis PMFL inspection probe system for the detection and characterization of defects in pipeline structures with more complex surface geometries than those investigated on this paper. Also the influence of neighboring defects on the detectability of surface and far-surface hairline cracks will be explored.

REFERENCES

1) U.S Department of Transportation, "Pipe Defects and Anomalies (pipeline & safety administration", [Online]. Available at: http://primis.phmsa.dot.gov/comm/FactSheets/FSPipeDefects.htm?nocache=9047. [Accessed 18 November 16].
2) M. Boat, N. Pearson, R. Lieb, J. Davies, R. James and B. Woodhead, "Factors that affect the defect sizing capabilities of the Magnetic Flux Leakage Technique", *Silverwing (UK) Ltd*, (2012).
3) H. M. Kim, D. W. Jeong, S. H. Im. J. H. Park, J. S. Lee and G. S. Park, "A Study on the Estimation of Defect Depth in MFL type NDT System", IEEE Transactions 40(2), 663–666 (2004).
4) Y. Shi, C. Zhang, R. Li, M. Cai and G. Jia, "Theory and application of magnetic flux leakage pipeline detection". *Sensors* 15(12), 31036-31055 (2015).
5) A. Sophian, G .Y. Tian, and S. Zairi, "Pulsed Magnetic Flux Leakage Techniques for Crack Detection and Characterization". *Sensors and Actuators A: Physical* 125(2), 186-191 (2006).
6) H. M. Kim and G. S. Park, "A Study on the Estimation of the Shapes of Axially Oriented Cracks in CMFL Type NDT System". *IEEE Trans*. Magn, 50 (2014).
7) P. J. Qing and J. A. Zhi, "Internal and external defect identification of pipelines using the PSO-SVM method. *Insight Non-Destruct*. Test. Cond. Monit, 57, 85–91 (2015).
8) H. M. Kim et al, "A Study on the Estimation of Defect Depth in MFL type NDT System". *School of Electrical Engineering, Pusan National University, Busan, South Korea*, gspark@pusan.ac.kr (2014).
9) H. M. Kim, and G. S. Park, "A Study on the Estimation of the Shapes of Axially Oriented Cracks in CMFL Type NDT System". *IEEE Transactions on Magnetics* 50(2), 109-112 (2014).
10) Y. D. Wang, Y. T. Xu, B. Wang, S. B. Ding, J. L. Xu and M. L. Zheng, "Research on metal atmospheric storage tank inspection method for standard in China". In Proceedings of the ASME 2009 *Pressure Vessels and Piping Division Conference, Prague, Czech Republic*, 447–452 (26–30 July 2009).
11) K. Hwang, "3-D defect profile reconstruction from magnetic flux leakage signatures using wavelet basis function neural networks". Electrical Engineering (Communications and Signal Processing*) PhD Thesis Lowa State University*, (2000).
12) J. Wilson and G. Y. Tian, "Pulsed Electromagnetic Methods For Defect Detection And Characterization". *NDT & E International* 40(4), 275-283 (2007).
13) L. Yong, J. Wilson, and G. Y. Tian, "Experiment and Simulation Study of 3D Magnetic Field Sensing For Magnetic Flux Leakage Defect Characterization". *NDT & E International* 40(2), 179-184 (2007).
14) Z. Y. Du and J. J. Ruan, "3-D FEM Simulation of Velocity Effects on Magnetic Flux Leakage Testing Signals". *IEEE Trans. Magn* 44, 1642–1645 (2008).
15) M. S. Safizadeha and T. Azizzadeh, "Corrosion detection of internal pipeline using NDT optical inspection system". *NDT&E Int.* 52, 144–148 (2012).
16) G. Y. Tian, J. Wilson, M. Morozov, D. O. Thompson and D. E. Chimenti, "Complementary electromagnetic Non-destructive évaluation". *AIP Conf. Proc*. 1335, 1256 (2011).
17) S. Mukhopadhyay and G. P. Srivastava, "Characterisation of metal loss defects from magnetic flux leakage signals with discrete wavelet transform", *NDT&E Int*. 33 (1), 57–65 (2000).
18) J. Fei, G. Tian, X. Zuo, Y. He, G. Tian and T. Zhang, "Extraction of Characteristic Quantity of Shallow Defects in Pulsed Magnetic Flux Leakage Signal", *Automation and Computing (ICAC)*, 2011 17th International Conference. [Online]. Available at: http://ieeexplore.ieee.org/abstract/document/6084931/. [Accessed: 24- Jan- 2017].
19) M. Katoh, N. Masumoto, K. Nishio and T. Yamaguchi, "Modelling of the yoke-magnetization in MFL-testing by finite elements", *NDT&E Int*.36 (7), 479–486 (2003).